crystals

MDPI

Article

Phase Composition and Temperature Effect on the Dynamic Young's Modulus, Shear Modulus, Internal Friction, and Dilatometric Changes in AISI 4130 Steel

Lioudmila A. Matlakhova [1,*], Emanuel C. Pessanha [1,2], Henrique Alves [3], Natalia A. Palii [4] and Sergio N. Monteiro [5]

1 Advanced Materials Laboratory, Science and Technology Center, Darcy Ribeiro State University of Northern Rio de Janeiro (UENF), Campos dos Goytacazes 28013-602, RJ, Brazil; emanuelcpessanha@gmail.com
2 Department of Chemical and Materials Engineering, Pontifical Catholic University of Rio de Janeiro (PUC-Rio), Rio de Janeiro 22453-900, RJ, Brazil
3 ATCP Physical Engineering, Ribeirao Preto 14026-567, SP, Brazil; ha@atcp-ndt.com
4 Laboratory of New Metallurgical Processes and Alloys, A. A. Baikov Institute of Metallurgy and Materials Science, Russian Academy of Sciences, 119334 Moscow, Russia; palii@imet.ac.ru
5 Department of Materials Science, Military Institute of Engineering (IME), Rio de Janeiro 22290-270, RJ, Brazil; snevesmonteiro@gmail.com
* Correspondence: lioudmila@uenf.br

Abstract: Elastic properties of materials and their changes with temperature are important for their applications in engineering. In the present study the influence of phase composition and temperature of AISI 4130 alloy on Young's modulus (E_d), shear modulus (G_d), and damping (Q^{-1}) was carried out by the impulse excitation technique (IET). The material characterization was performed using confocal microscopy, XRD, SEM, HV, and dilatometry. A stable structure, composed of ferrite (BCC) and pearlite (α-Fe + Fe_3C), was obtained by annealing. Metastable structure of martensite (BCT) was obtained by quenching. The E_d, G_d, and Q^{-1} were measured by varying the temperature from RT to 900 °C. The values of E_d and G_d, at RT, were determined as 201.5 and 79.2 GPa (annealed) and 190.13 and 76.5 GPa (quenched), respectively. In the annealed steel, the values E_d and G_d decrease linearly on heating up to 650 °C, with thermal expansion. In the quenched steel, weak changes occurred in the dilatometric curve, E_d, G_d, and Q^{-1}, in the range of 350–450 °C, which indicated decompositions of the martensitic phase. A sharp decrease in the moduli and high peak of Q^{-1} were observed for both samples around 650–900 °C, revealing low lattice elastic stability of the phases during transformations α(BCC) + Fe_3Cγ(FCC).

Keywords: elastic properties; low-alloy steel; heat treatment; structural stability; martensitic phase; phase transformation; impulse excitation technique

check for updates

Citation: Matlakhova, L.A.; Pessanha, E.C.; Alves, H.; Palii, N.A.; Monteiro, S.N. Phase Composition and Temperature Effect on the Dynamic Young's Modulus, Shear Modulus, Internal Friction, and Dilatometric Changes in AISI 4130 Steel. *Crystals* **2023**, *13*, 930. https://doi.org/10.3390/cryst13060930

Academic Editor: Hongbin Bei

Received: 10 May 2023
Revised: 27 May 2023
Accepted: 1 June 2023
Published: 9 June 2023

1. Introduction

The elastic properties of alloys are fundamental characteristics associated with the atomic binding energy and are determined by small deviations of the atoms from their equilibrium positions. The modulus of elasticity, or Young's modulus (E), is related to the alloy's stiffness and is an intrinsic property of each material. The shear modulus, or modulus of rigidity (G), describes the resistance of the material to a shearing deformation in the elastic regime [1,2].

The AISI 4130 is a low-alloyed Cr-Mo carbon steel that is widely used in buildings, aircraft, as well as automotive industries as structural steel. It is also used in machinery parts, for instance, gears, drill bits, cutters, mills, etc. [3–8]. The AISI 4130 steel microstructure and properties are very sensitive to heat treatment. A stable and metastable microstructure composition can be easily attained by annealing and quenching heat treatments, respectively. For instance, excellent ductility (25.5%) is presented by AISI 4130 in the annealed state. On the other hand, by heat treatment, an ultimate tensile strength limit of up to

~1100 MPa can be achieved [8,9]. As a structural steel, the E of the AISI 4130 steel is the main property to be well understood. In some of the above-mentioned applications, the stiffness variation with temperature increasing is of great importance, in the material that could undergo heating during its use. However, as far as the authors are aware, there are no previous studies on the elastic properties' behavior during the heating of this alloy. Therefore, understanding the behavior of E, G, and Q^{-1} as well as the phase stability of AISI 4130 steel during heating and cooling cycles is of great relevance for new projects, which use this alloy, to be developed.

The qualitative methods commonly used to determine elastic properties of metal alloys are destructive and have geometry restrictions, i.e., need standard samples and qualified staff for subsequent data analysis. A typical example is the widely applied tensile test by the quasi-static loading with a total deformation exceeding 1% [2].

In contrast to quasi-static methods, the dynamic testing methods for elastic-strength characteristics, including dynamic Young's modulus (E_d), dynamic shear modulus (G_d), and Poisson's ratio (μ), operate by means of excitation of atomic vibrations through the propagation of elastic waves and by the determination of the resonant frequencies of lattice vibration of the materials without causing plastic deformation. These methods are of high precision. Moreover, they justify the use of resonance methods for the study of various types of phase transformations in steels and alloys over a wide temperature range. Electromagnetic, piezoelectric, electrostatic, electrodynamic, mechanical, and other methods can also be used to excite vibrations in the sample for the determination of the dynamic modulus of elasticity [10]. Nowadays, many researchers are using ultrasonic and impulse excitation techniques as non-destructive testing to evaluate the mechanical properties of metallic materials [2,10–17].

In particular, the impulse excitation technique (IET) has been highlighted as a straightforward, non-destructive, and fast method for the determination of the elastic constants and damping characteristics of different classes of materials [12–16]. The IET is based on the acoustic response in free vibration, after an initial impulse, of the material whose elastic properties are to be determined [17].

The stability of the elastic properties at different temperatures will affect the application of the material in harsh environments. For example, the natural frequency of some special engineering designs changes with the temperature. Therefore, metals and alloys with more stable elastic properties are desirable in engineering applications. Furthermore, sometimes engineers are interested in the elastic constants of a new metal alloy. Especially in reverse engineering, material properties need to be measured without sample destruction. Thus, the non-destructive approach is advantageous for material characterization [18–22].

The importance of studying the elastic properties became particularly evident when Zener [23] found that in the ordered body-centered cubic (BCC) phases of the CsCl type, the shear modulus in the crystallographic systems (110) decreased in value, which led to the loss of elastic stiffness and subsequent phase transformation. It has been found that in polycrystalline alloys undergoing reversible martensitic transformation (RMT), both E and G decrease and pass through a minimum, indicating a loss of elastic stiffness and rigidity of the martensite lattice upon heating. With the formation of the high-temperature phase (austenite), the elastic stability of the lattice increases, i.e., its stiffness and rigidity increase, and as a result the E and G increase again.

This drop in the E and G to a minimum value (softening) has been observed both on heating to A_s (associated with the reverse martensitic transformation M→A) and on cooling to M_s (associated with the direct martensitic transformation A→M) in quenched alloys of Au-Cd [24], In-Tl [25], Mn-Cu [26], β-Cu-Au-Zn [27], TiNi [28] and other systems. In the critical interval of phase transformations, Poisson's ratio reaches the highest values [24,28,29]. On completion of the phase transitions, the moduli increase again [24,27–29].

Therefore, measurements of E and G are of great help in studying phase transformations in steels. Anomalous behavior of the elastic properties was also found in Fe-based alloys with RMT: Fe-Cr-Ni, Fe-Mn, Fe-Ni-Co-Ti [30], carbon steels, and stainless steels [16,19–22,31].

In their study, Popov and Shitikova [16] aimed to gain more insights into complex processes that take place in quenched and tempered steels with different chromium contents (3%, 12%, and 18 wt.%), by measuring the E_d and the hardness. The values of E_d were determined by the dynamic method by comparing the natural frequency of the vibrations with the frequency of a string stretched by a weight. They found that the E_d of high-alloy chromium steels begins to increase after low-temperature quenching and then remains almost constant up to quenching temperatures of 525–550 °C. The higher the Cr content of the steel, the smaller the initial increase and the longer the horizontal part of the curve. It can be seen that a small peak occurs at 150 °C and then the hardness starts to drop. Another peak was observed at 450–500 °C, because of participation of the carbide phase. After quenching and tempering at 525–550 °C, the hardness decreases and E_d increases up to 700 °C.

Lindgren and Back [19] aiming to simulate several thermo-mechanical processes, proposed: "a model for hypoeutectoid steels that accounts for temperature dependency as well as the influence of alloying. The model consisted of separate parts for the ferrite and austenite phases. The latter also included a specific contribution due to ferromagnetism. The model was calibrated versus iron and evaluated against various low alloy steels".

In a recent investigation of Tripathy et al. [22] high-temperature E_d of an advanced 18Cr-9Ni-2.95Cu-0.58Nb-0.1C austenitic stainless steel was measured during heating to 1000 °C and cooling to room temperature (RT) using the IET. The E_d and G_d values in the heating cycle were found to decrease with increasing temperature with a non-linear behavior. It was also found that during cooling the Cu precipitation from the austenite matrix contributed to the significant moduli variations at 689–477 °C, indicating instability, decomposition, and change in austenite phase composition in this thermal interval.

In the study of Fukuhara and Sanpei [31] the temperature dependence of the E_d, G_d, and bulk moduli, Poisson's ratio and the Lamé parameter, as well as longitudinal and transverse internal friction values for low-carbon steel S10C and stainless steel SUS304 were measured simultaneously over a temperature range of 300–1500 K using an ultrasonic pulse sing-around method. The authors indicate that the E_d and G_d decrease while Poisson's ratio increases with increasing temperature, suggesting activation of the shear mode in the high-temperature region. It was found that the internal friction was sensitive to the recrystallization process, to α(ferritic)→γ(austenitic) phase transformation, and to the dissolution of precipitated carbide phases into the austenitic matrix, respectively.

Indeed, there are few data on the temperature behavior of the elastic moduli and damping characteristics of low-alloy carbon steels, which are widely used in engineering applications. On the other hand, these steels are sensitive to the heat treatments that are applied and show structures with both stable and metastable phases.

It is well known that tempering of quenched steels is accompanied by the decomposition of the α- and γ-solid solutions and also by carbide transformations. The processes that occur within steels are very complex. Taking into account that the elastic properties are very sensitive to phase composition and to distortions of the crystal lattice, the measurement of the E_d and other properties, with quenching and tempering, is useful for the study of structural changes in heat-treated steels.

For scientific and technical purposes, it is important to obtain and compare the values of the E_d, G_d, Q^{-1}, as well as their changes with temperature, for low-alloy carbon steels with stable and metastable structures as a result of different heat treatments. Consequently, studies on the feasibility of the IET to assess the dynamic elastic properties associated with the phase stability of low-alloy steels, as temperature varies continuously, are timely and relevant.

This work aimed to study the dynamic elastic moduli and damping behavior in AISI 4130, as a function of temperature, and to correlate their changes with phase stability in this alloy with different initial structures: stable (annealed) and metastable (quenched), as a result of heat treatment. As far as the authors are aware, this is the first investigation of AISI 4130 elastic properties and phase stability as a function of temperature carried out by means of the IET.

2. Materials and Methods

The AISI 4130 steel was produced by Villares Metals S/A and was supplied by the IST Supply Commercial EIRELI, Brazil. Table 1 presents the nominal composition of the used specimen.

Table 1. Chemical composition (wt.%) of AISI 4130 (IST Supply Commercial EIRELI).

C	Mn	Si	P	S	Cr	Ni	Mo	V	Al	Cu	N	Fe
0.3	0.54	0.23	0.006	0.008	0.86	0.25	0.19	0.01	0.019	0.09	0.005	rest

The AISI 4130 samples for E_d, G_d, μ, and Q^{-1} determination had a rectangular cross-section with the dimensions 150 mm × 25 mm × 10 mm. The dimensions were defined based on the dimensional criteria for the IET and in accordance with the ASTM E1876-22 standard [10], which is based on the material's acoustic response to impulse excitation. The samples were split into two batches. One batch was annealed and the other was quenched. Both the annealing and quenching treatments were carried out in a box furnace according to the conditions given in Table 2.

Table 2. AISI 4130 alloy specimen heat treatment parameters.

	Annealing	Quenching
Temperature	860 °C	870 °C
Soaking time	1 h	1 h
Cooling	Slow (in the furnace)	Fast (cold water)

Microstructural observation by confocal microscopy (CM) was carried out, after a conventional metallographic preparation, with the OLYMPUS LEXT OLS4000 microscope for morphological characterization of the obtained microstructures. Hereafter, scanning electron microscopy (SEM) was carried out with a SHIMADZU SSX-550 microscope for a more detailed microstructural and morphological analysis of the specimens.

X-ray diffraction (XRD) was performed on a Bruker D8 DISCOVER using Cu Kα radiation (λ = 0.15418 nm) to determine the phase composition of the annealed and quenched sample. The data were acquired in the 2θ range from 40° to 100° with a step size of 0.03° and a counting time of 3 s per step.

Vickers hardness tests were carried out in a digital microhardness machine (Time Group Inc.®, Beijing, China) with an applied load of 10 kgf. Ten microhardness measurements were performed in each sample. The results obtained were statistically processed.

Dilatometric analysis was carried out to track critical temperature intervals for phase decomposition and phase transformations. Dilatometric curves were recorded, from room temperature (RT) to 900 °C at a rate of 5 °C·min^{-1}, by a DIL 402C-NETZSCH dilatometer.

During the IET measurements, an impulse excitation was provided by a brief impact on the sample. This impact generates vibrations that are intrinsic to each material and sample, also known as the natural frequency of vibration, and are temperature dependent. These vibrations are picked up by a microphone. In situ measurements were made during the heating and cooling cycles of the samples at temperatures ranging from RT to 900 °C. In accordance with ASTM E1876-22 [17] Equations (1) and (2) were used for the determination of E_d and G_d of an excited bar with a rectangular section.

$$E = 0.9465\left(\frac{m \times f_f^2}{b}\right)\left(\frac{L^3}{t^3}\right)T_1 \quad (1)$$

$$G = \left(\frac{4 \times L \times m \times f_t^2}{b \times t}\right)\cdot R \quad (2)$$

where E_d is the dynamic Young's modulus [Pa], G_d is the dynamic shear modulus [Pa], m is the bar mass [g], b, L, and t are the bar width, length, and thickness [mm], respectively, while f_f is the bar natural resonant frequency in bending [Hz], f_t is the bar natural resonant frequency in torsion [Hz], T_1 and R are correction factors.

Damping causes mechanical energy dissipation. In the case of the IET, the energy is that of the acoustic wave, generated by the initial pulse, propagating in the analyzed material. Therefore, the damping was evaluated by the internal friction (Q^{-1}) of the studied steel sample, using the logarithmic decrement method according to Equation (3).

$$Q^{-1} = \frac{\delta}{\pi}; \qquad \delta = ln\left(\frac{A_n}{A_{n+1}}\right) \quad (3)$$

where d is the logarithmic decrement, while A_n and A_{n+1} are the amplitude of two successive cycles [17,32,33].

The Sonelastic® software 5.0, developed by ATCP Physical Engineering (Ribeirão Preto, SP, Brazil), was used to process the obtained data [17].

3. Results and Discussion

The results of microstructural analyses of AISI 4130 by CM and SEM are shown in Figures 1 and 2. The microstructure of annealed AISI 4130 (Figure 1) is composed of equiaxed grains of primary ferrite (α-Fe) and of the lamellar component pearlite (α-Fe + Fe_3C). The microstructure of the same quenched alloy is predominantly martensite with characteristic lamellar morphology, but some retained austenite can also be present (lighter areas in Figure 2a). The microstructures observed are typical for annealed and quenched low-alloyed hypoeutectoid carbon steels [34–36].

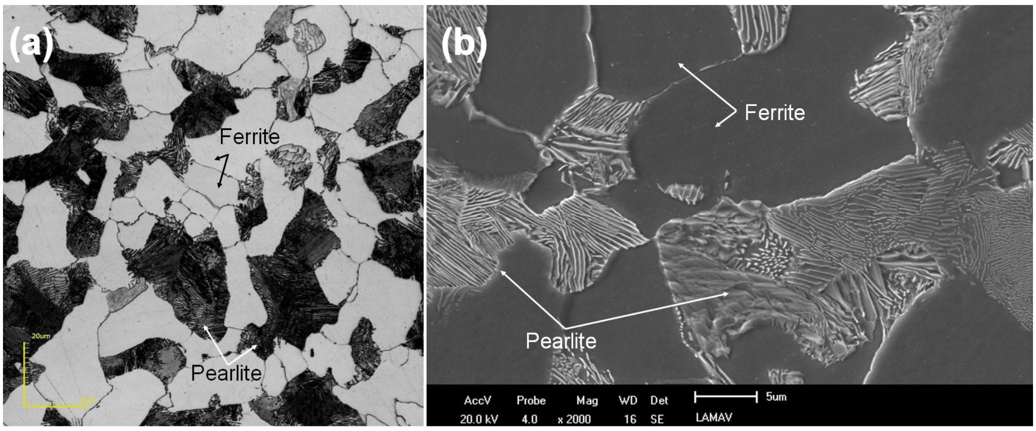

Figure 1. Images of: (**a**) confocal microscopy (scale bar = 20 μm) and (**b**) scanning electron microscopy of annealed AISI 4130 (scale bar = 5 μm).

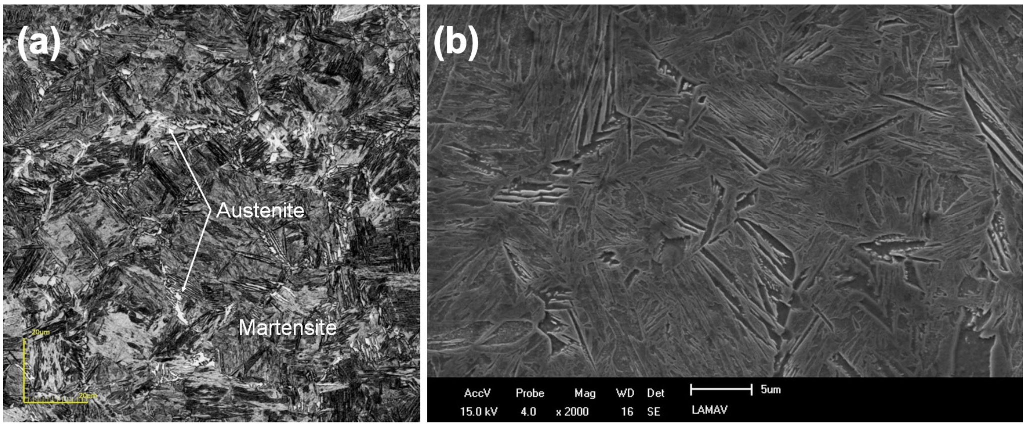

Figure 2. Images of: (**a**) confocal microscopy (scale bar = 20 µm) and (**b**) scanning electron microscopy of quenched AISI 4130 (scale bar = 5 µm).

Figure 3 shows the experimental XRD patterns of annealed and quenched AISI 4130. In the annealed state (Figure 3a) it was possible to determine the body-centered cubic (BCC) ferrite phase by strong diffraction peaks of its crystal planes: $(110)_\alpha$, $(200)_\alpha$, $(211)_\alpha$, and $(220)_\alpha$, compared with [37,38]. The presence of cementite Fe_3C (rhombohedral, oP16), was detected by diffraction peaks of its crystal planes: $(211)_{Fe3C}$, $(122)_{Fe3C}$, $(301)_{Fe3C}$, $(331)_{Fe3C}$, $(133)_{Fe3C}$, $(400)_{Fe3C}$, compared with the data of [39].

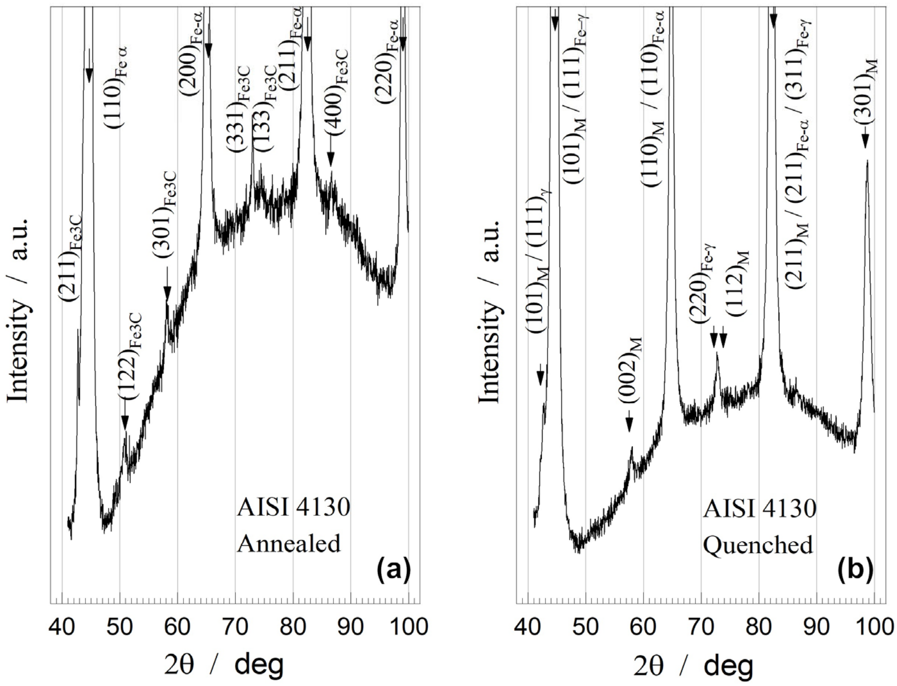

Figure 3. XRD patterns for (**a**) annealed and (**b**) quenched AISI 4130 samples.

The XRD pattern of the quenched sample (Figure 3b) reveals the major presence of the martensite, with the body-centered tetragonal (BCT) structure, determined by very weak diffraction peaks of its crystal planes: $(101)_M$, $(110)_M$, $(002)_M$, $(200)_M$, $(112)_M$, $(211)_M$, $(103)_M$, $(301)_M$, compared with the data of [40].

A certain shift of the martensite peaks towards lower 2θ angles and larger lattice parameters, as compared to the corresponding peaks of the ferrite structure, indicates a distortion of the cubic lattice towards a BCT one. However, this distortion is not very pronounced due to the low carbon content (0.3 wt.%) in the steel. In addition to martensite, the small amount of face-centered cubic (FCC) retained austenite in the quenched steel was identified by very weak peaks of the planes $(111)_\gamma$, $(200)_\gamma$, $(220)_\gamma$, $(311)_\gamma$, $(222)_\gamma$ [41]. It is possible to observe that a large part of the austenite has undergone a transformation during the quenching process. The XRD results, for both annealed and quenched samples, are in agreement with the observed microstructures (Figures 1 and 2).

The chemical composition and structure are correlated with the hardness of the alloys. The Vickers hardness for AISI 4130, after heat treatments, was determined to be 160 ± 15 kgf/mm^2 for the annealed state and 541 ± 46 kgf/mm^2 for the quenched state, i.e., the hardness in the quenched sample increased more than three-fold compared to the annealed one (Table 3). It is important to emphasize that the crystal lattices of the austenite and martensite, which are simultaneously present in the steel microstructure, are interconnected by orientation relationships. Indeed, the lattice planes of austenite and martensite, which have certain crystallographic indices, are parallel to each other. In the transformation $\gamma_{Fe} \rightarrow \alpha_{Fe}$ the $(111)\gamma$ planes are parallel to $(110)\alpha$ where the $[110]\gamma$ directions are parallel to $[111]\alpha$. In carbon steel, the habit planes for martensite are the $\{225\}\gamma$ and $\{259\}\gamma$ planes. In carbon steel, the austenite is a solid solution of carbon and alloying elements. During the quenching, the metastable FCC austenite is prone to reject the 0.8 wt.% C held in solid solution because of the stable BCC α-Fe solubility limit (0.01 wt.% C).

However, on the fast cooling, the temperature drops so quickly that the carbon atoms do not have time to diffuse out of the austenite lattice. At a critical temperature interval, the diffusion process results in a highly strained BCT martensite that is supersaturated with these elements. The presence of intrinsic atoms at levels above the solubility limit of the BCC ferrite determines its BCT distortion. Moreover, the shear deformations that arise produce a large number of dislocations, which is a primary strengthening mechanism of steels [42–45].

Dilatometric curves for the annealed (Figure 4a) and quenched (Figure 4b) samples showed positive extrinsic coefficient of thermal expansion (CTE) up to 760 °C.

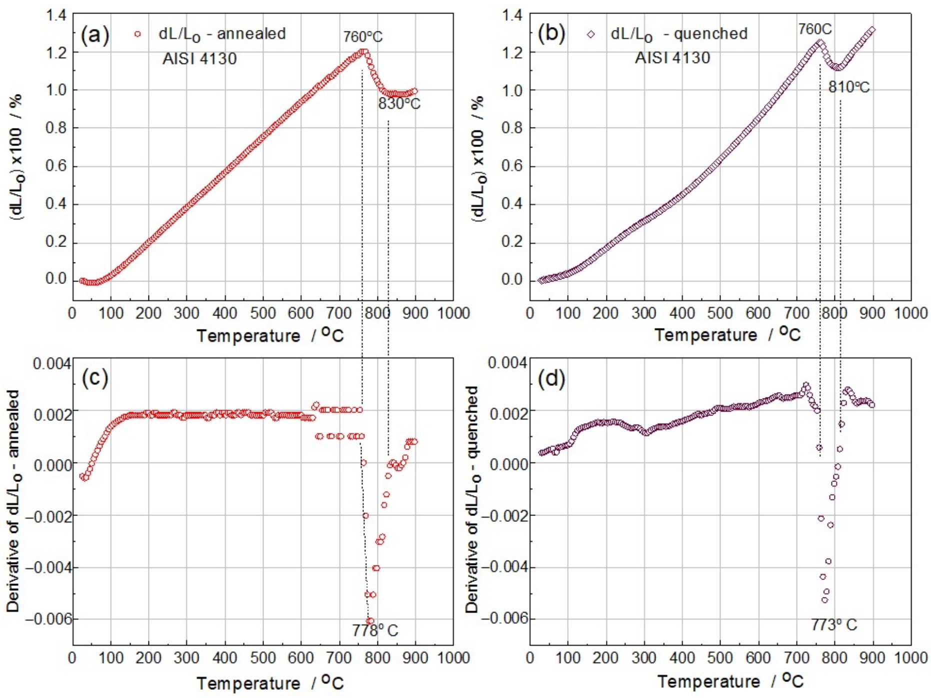

Figure 4. Dilatometric curves and first derivatives for (**a**,**c**) annealed and (**b**,**d**) quenched samples of AISI 4130 (v = 5 °C.min^{-1}).

However, different trends in the CTE with increasing temperature were observed for each sample. While the CTE for the annealed sample shows a linear behavior up to 760 °C (Figure 4a,c), which is the expected temperature for the onset of austenite formation from ferrite and cementite [36,42,46–51], the CTE for the quenched sample shows a non-linear behavior in the interval from 100 to 300 °C. In this interval, the decomposition of martensite can be expected, as observed in similar systems [47,48] with the formation of ferrite and cementite and the decomposition of retained austenite at higher tempering temperatures, accompanied by slight expansion and compression of the sample, as shown in Figure 4b,d.

According to the dilatometric curves in Figure 4, it might be expected that in the annealed sample the initial phase composition would be stable up to 750 °C. Otherwise, in the quenched sample, the structural stability would only be achieved above 600 °C, with the formation of stable ferritic and cementite phases within the refined sorbite. On further heating, these phases can undergo coalescence, grain growth, and it transform into a spherite structure, which persists up to 750 °C.

With respect to temperatures above 760 °C, both samples exhibit a volume contraction, which would be caused by the formation of austenite from ferrite and cementite phases [36]. Since austenite has a higher atomic packing factor than ferrite [49], this macroscopic volume contraction is attributed to lattice shrinkage.

During austenitization, complex phase transformations occur in this temperature range, including the phase transformation from ferrite to austenite, the dissolution of cementite (carbide), the diffusion of carbon and alloying elements, and the saturation of the jointly formed austenite [52,53]. The diffusion process depends on the temperature, the chemical composition, the alloying elements, and the size of the constituents involved.

The evolution of this process is different for the two studied materials. The annealed sample suffered compression from 760 °C up to 820 °C, then remained roughly constant and unchanged up to 900 °C, showing a plateau on the dilatometer curve. This plateau indicates that the diffusion processes of austenitization do not stop at 830 °C and continue at higher temperatures, compensating for the positive effect of lattice thermal expansion.

On the other hand, in the initially quenched sample, the compression temperature range is narrower. It quickly exhibits a positive and linear extrinsic thermal expansion of the newly formed austenite phase from 810 °C. It is expected that at 830 °C the structure of both alloys consists of an austenite phase. However, in the quenched alloy, the dissolution and homogenization processes seem to be more complete in this interval, due to the more quickly refined microstructure. As a result, the austenite formed is more stable, more homogeneous, and exhibits normal thermal expansion on subsequent heating.

The values of E_d, G_d, μ, and Q^{-1}, derived from the torsional frequency of annealed and quenched AISI 4130 steels, were determined at RT and during heating and cooling cycles, as a function of temperature.

The results of the RT measurements are given in Table 3. The values of the dynamic moduli for the two different initial states are very close, but there is a tendency for the dynamic elastic property values of the quenched alloy to be lower with metastable martensitic structure.

Table 3. Values of dynamic elastic moduli E_d, G_d, μ, and Vickers hardness of AISI 4130 in annealed and quenched samples.

Condition of AISI 4130	E_d (GPa)	G_d (GPa)	μ	HV (kgf/mm^2)
Annealed	201.5 ± 1.9	79.2 ± 1.1	0.27	160 ± 15
Quenched	190.1 ± 4.6	76.5 ± 0.9	0.27	541 ± 46

These dynamic moduli results are compatible with other frequency resonance data [31] obtained in a normalized low-carbon steel S10C with 0.12 wt.% C: 206.6 GPa (E_d) and 80.7 GPa (G_d), at RT.

For both annealed and quenched samples, there is an approximately linear decrease from RT to 600 °C for both E_d and G_d moduli (Figures 5 and 6). Due to the positive coefficient of thermal expansion in this temperature range, the higher the temperature, the higher the atomic bonding vibration amplitude, the greater the atomic distance, and the weaker the interatomic bonds [54]. Therefore, the decrease in these dynamic moduli can be attributed to the softening of the bonds as a result of the increase in temperature.

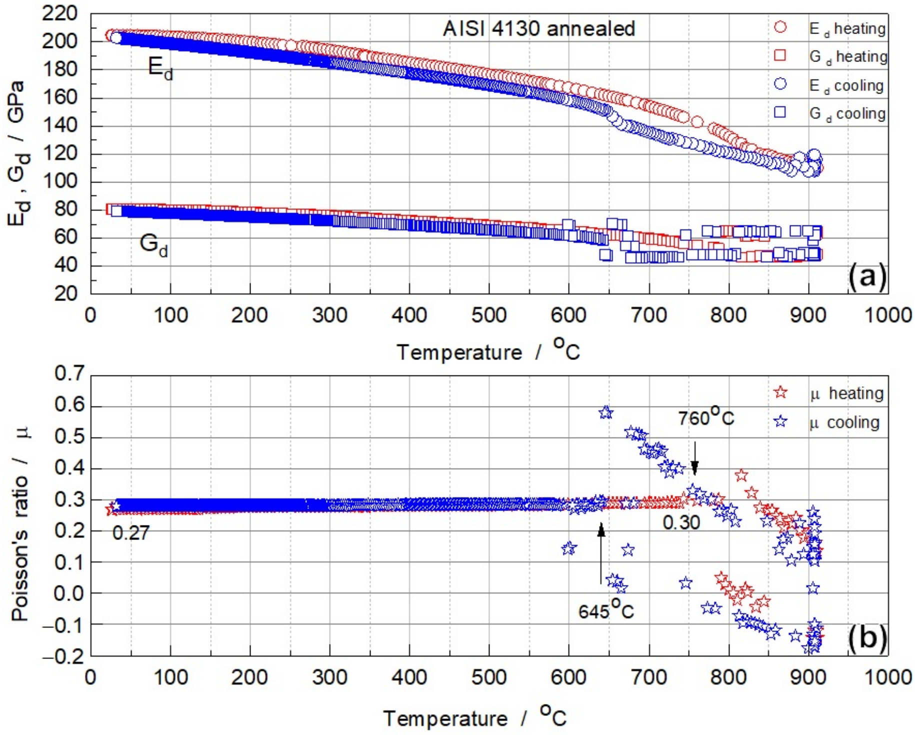

Figure 5. (**a**) Moduli E_d, G_d and (**b**) Poisson's ratio μ of annealed AISI 4130 specimen during heating and cooling.

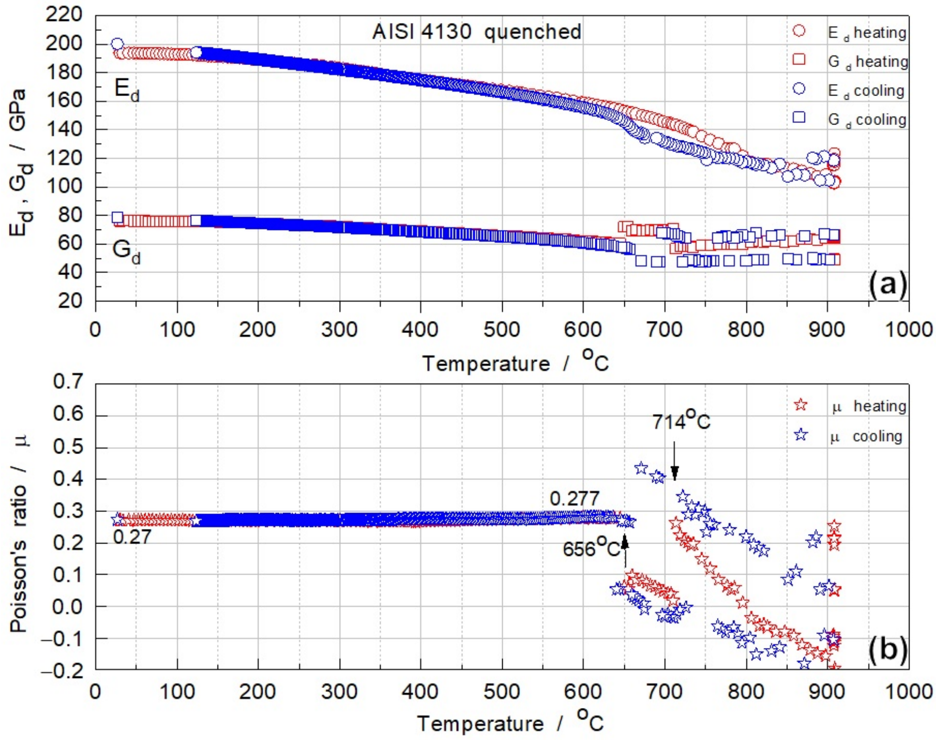

Figure 6. (**a**) Moduli E_d, G_d and (**b**) Poisson's ratio μ of quenched AISI 4130 specimen during heating and cooling.

In both cases, dynamic moduli E_d and G_d begin to decrease more sharply above 600 °C, dropping rapidly above 750 °C, indicating loss of elastic stability of ferrite and austenite lattices in the transformation interval [27–29]. These dynamic moduli changes agree well with dilatometric analysis results (Figure 4).

It should be noted that in the critical temperature range, when the sample becomes heterogeneous in structure, i.e., with different parts, the heated part transforms more rapidly and has a different phase composition than the less heated part. This could explain the reason why the values of G_d begin to overlap. In this case, the impact produces a characteristic heterogeneous structure vibration. This effect, when using the IET, has been described in detail in [54]. However, the natural vibrations that characterize modulus E_d are less susceptible to this phenomenon.

On cooling, the anomalous change in the dynamic moduli shows an interval of phase transformation from austenite to primary ferrite and eutectoid ferrite + cementite mixture (pearlite). Below 600 °C the modulus changes almost linearly due to the temperature effect of reduction of the bonds' vibration amplitude when cooling down.

It can be noted that a hysteresis was observed in both samples, i.e., the sharp change in E_d was observed around 750 °C during heating and around 650 °C during cooling. This hysteresis could be related to the supercooling required for the phase transformation, which would occur in a time-dependent phase transformation [55,56].

The μ of annealed and quenched alloys, of 0.27 at RT, increased slightly on heating to 750 °C to 0.28 (hardened alloy) and 0.30 (annealed alloy) (Figures 5 and 6). This is typical of most steels [56,57]. However, when complex phase transformation processes between thermodynamically stable phases start in an alloy, the Poisson's ratio changes drastically and becomes negative, which is characteristic of many anisotropic crystals [33,58,59].

In the cooling cycle, starting at 900 °C, μ increases, reaching critically high values (0.5) at 645 °C, and then drops sharply to 0.29, at the end of the phase transformation. These anomalous changes have been observed for alloys with two different initial states. However, it should be emphasized that the phase composition of these alloys is identical until phase transformation occurs during austenitization.

Particular attention has been paid to the temperature variation of E_d of the alloys. Figure 7 compares the behavior of E_d, of annealed (Figure 7a) and quenched (Figure 7b) samples as a function of temperature, during heating and cooling cycles.

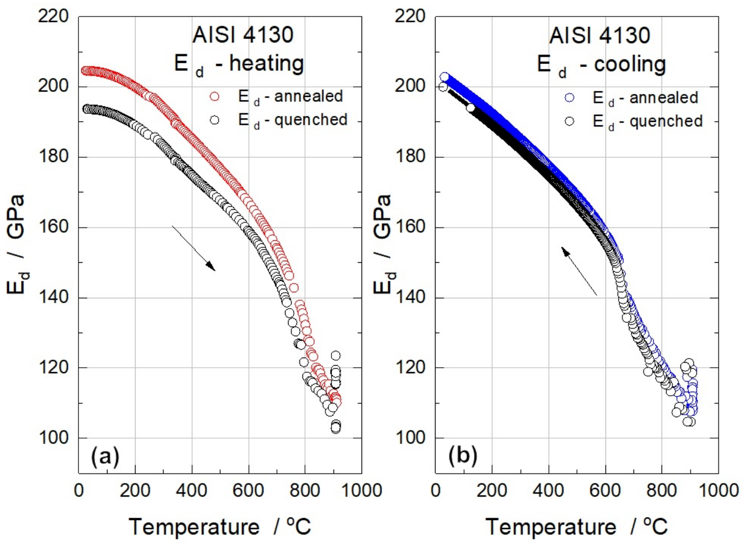

Figure 7. E_d of annealed and quenched samples of AISI 4130 during (**a**) heating and (**b**) cooling cycles, the arrows indicate the course of the temperature change.

A comparative analysis demonstrates that the behavior of E_d is quite similar for annealed and quenched steels with different initial structures. In the quenched alloy, the process of martensite decomposition and transformation of the residual austenite phase into supersaturated ferrite takes place in the range 200–350 °C and is characterized by a slight change in the slope of the monotonic modulus decrease curve. The E_d values converge at higher temperatures, which is an indirect indication of the already identical phase composition of the two samples. Above 650 °C, the E_d of both samples changes the slope of its temperature dependence, dropping almost identically up to 850 °C, reaching 120–130 GPa. It is known that the value of E_d and G_d decreases at the threshold of phase transformation and especially at the time of transformation, indicating a loss of elastic stability of the initial alloyed structure [27–29]. Interestingly, the phenomenon of softening and loss of elastic stability in this case occurs in a system where phase transformation between stable phases is expected. The material structure is represented by an austenitic phase above 850 °C. According to the dilatometry results, the change in the slope of E_d between 850 and 900 °C can be explained by the fact that austenite is formed directly from sorbite in the previously quenched alloy over a narrower temperature range. The quenched sample showed greater homogeneity and greater lattice stability than the annealed sample, where the austenite had not yet reached chemical homogeneity and the stabilization process seems to be lazier. With stabilization, one would expect an increase in the value of E_d as a result of an increase in the elastic stability of the lattice, but the temperature factor is stronger and the process of decreasing the E_d continues, albeit with less intensity. A similar behavior of E_d was obtained by Fukuhara and Sanpei [31] where 0.12% C steel was heated from 23–1223 °C after normalization. The authors observed that: "The moduli of the carbon steel decrease substantially as the temperature increase. The modulus-temperature slope of Young, shear moduli change to more sluggish one at around 725 °C", and the changing of the slope of the E_d vs. temperature curve was interpreted as follows: "a possibility that the change is due to α(ferritic)→γ(austenitic) phase transformation".

Figure 8 shows the values of internal friction (Q^{-1}) of initial annealed and quenched AISI 4130 steel as a function of temperature, during heating and cooling cycles. Comparing the behavior of Q^{-1} with the elastic moduli of annealed and quenched steel samples, some similarities can be observed, but there are also differences.

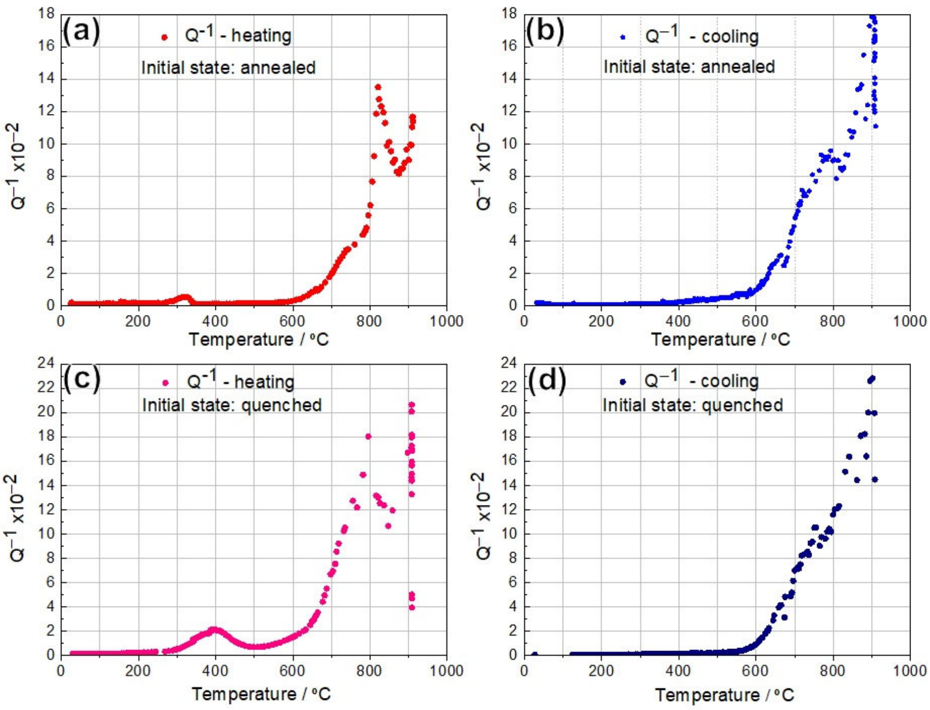

Figure 8. Values of internal friction (Q^{-1}) of AISI 4130 in (**a**,**b**) annealed and (**c**,**d**) quenched state, during (**a**,**c**) heating and (**b**,**d**) cooling.

The values of internal friction Q^{-1} for both materials studied are relatively lower at up to 250 °C with small changes in E_d and G_d. This may be due to the thermal stability of both the stable and metastable structures in this interval. (Figures 5–7). During heating of the annealed steel, the first, very low peak of Q^{-1} appears in the 250–350 °C range, which can be ascribed to the release of internal stresses and appears due to the dislocations movement in relaxation processes [60]. Hereafter, when heating up to 550 °C, Q^{-1} keeps low values, as a result of dislocation annihilation. The relaxed structure, with no significant changes, suffers an expansion on heating, and in this interval, the moduli change in a practically linear manner up to 600 °C.

Unlike the annealed state, in the quenched alloy, the first peak of internal friction Q^{-1} is wider, more intense, and appears in the 250–500 °C range, with its maximum at 450 °C.

In this temperature range, complex structural and phase transformation processes are expected to occur, which are characteristic of the tempering of carbon steel after quenching. They include: (i) interaction of dislocations with atmospheres of interstitial impurities, including carbon atoms; (ii) movement of dislocations to relieve internal stresses, decomposition of martensite with precipitation of metastable carbides (200 °C), their growth and transformation to more stable phase, decomposition (200–300 °C) of residual austenite; and (iii) its transformation to saturated ferrite and cementite (bainite). Above 400 °C, the recovery and recrystallization of stable α-ferrite (BBC) and formation of cementite in the form of sorbite and then spheroidite, a globular cementite in ferrite matrix, are to occur [52,61,62].

The peak's intensity is determined by the content of interstitial atoms in the solid solution and by the magnitude of the local internal microstrains in the initial martensite. In addition to the complex structural changes, the magnetoelastic component of the vibrations, which is characteristic of ferromagnetic materials, can be involved in the whole process of the internal friction [8,60].

However, the higher the internal friction, the higher the absorption capacity that was observed in alloys during their heating and cooling in the temperature range of phase transformations. Both internal friction and the absorption capacity are sensitive to heterogeneous structure states, when new crystal lattice grains are forming inside the parent phase, accompanied by the interphase boundary formation and movement, the atom displacement, the emergence of elastic deformations due to grain misfit, as well as the movement and generation of dislocations, in the conditions of loss of elastic stiffness and rigidity of transformed material [29,60].

Figure 9 shows the first-order temperature derivative (dE_d/dT) curves of the studied steel in the initial annealed and quenched states during heating and cooling. This practically linear decrease in E_d of the annealed alloy on heating and its increase on cooling in the range from 20 to 600 °C, associated with thermal expansion and contraction of the lattice (Figure 7), is confirmed by the practically linear behavior of its first derivatives, with a small deviation in the range from 200 to 300 °C (Figure 9). The linear behavior of the derivative curve is abruptly interrupted above 600 °C, when the material softens as it approaches the critical temperature range. It drops sharply to a minimum when heated to 800 °C and then rises sharply.

In contrast to the annealed alloy, when the quenched alloy is heated, the first derivative of E_d in the range 200–500 °C (Figure 9) shows a visible deviation from the linear relationship. Moreover, there is also an increase in the derivative, i.e., a slight increase in E_d, between 300 and 500 °C, which is hardly noticeable in the temperature change of E_d (Figure 7a). It should be noted that, in the temperature ranges in which the derivatives deviate from the linear relation E_d, the internal friction Q^{-1} shows the first peaks (Figure 8). The increase in modulus in the quenched alloy, in the range 300–500 °C, proves the phase transformation process, $\gamma \rightarrow \alpha'$, when residual austenite reversibly converts to martensite, which itself decomposes by the known mechanisms that form refined sorbite that subsequently suffers spheroidization to form globular cementite distributed in ferrite matrix [8,9,52].

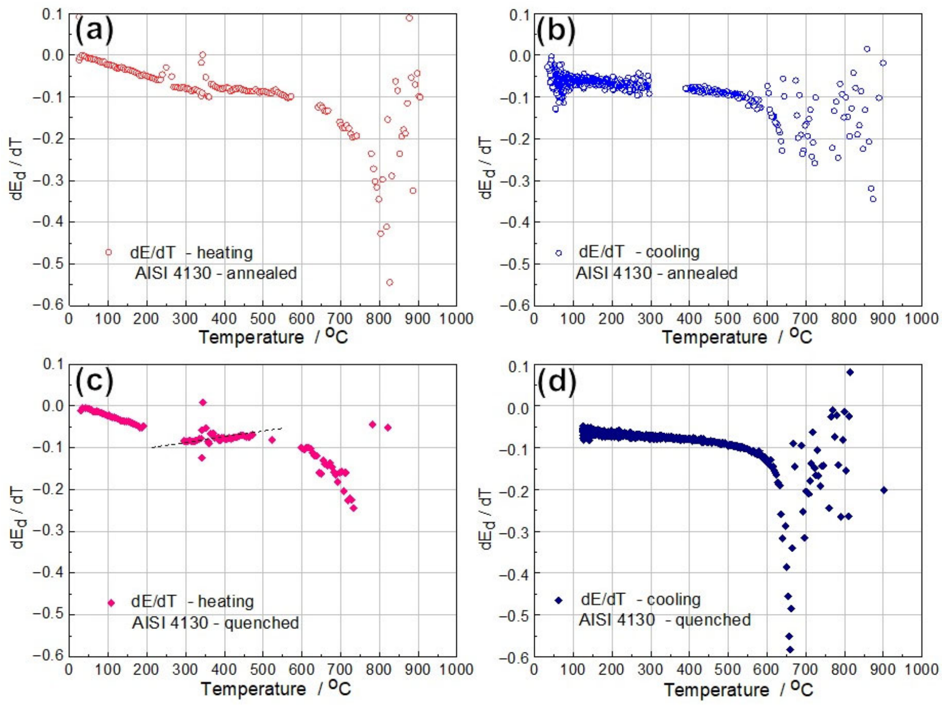

Figure 9. First-order temperature derivative (dE_d/dT) curves of AISI 4130 in the initial (**a**,**b**) annealed and (**c**,**d**) quenched states during (**a**,**c**) heating and (**b**,**d**) cooling.

On further heating above 600 °C, as in the case of the annealed alloy, the derivative of E_d decreases sharply. As the previously quenched alloy cools from 900 °C, the derivative of E_d drops to its minimum at 650 °C, and then rises sharply up to 600 °C. Below 600 °C the first derivative E_d increases almost linearly, which is consistent with the increase in the value of E_d. The linear behavior of the derivative on cooling below 600 °C is evidence that the phase and structural transformations produced by heating are irreversible.

It was shown that, consistent with the linear expansion of the studied steel, the values of E_d and G_d decrease smoothly and almost linearly on heating up to 650 °C. In the quenched state steel, with initial martensitic structure and traces of residual austenite, in the temperature range 350–450 °C, weak changes in the dilatometric curve and in the temperature behavior of the elastic moduli are observed. Together they indicate transformations occurring in the initial martensitic structure, typical of tempering, and its transformation into a sorbite structure with stable ferrite and cementite phases.

In samples with a different initial structure, the values of E_d and G_d show a more pronounced decrease upon heating above 650 °C, indicating a pre-transition state. The similar behavior of dynamic elastic moduli, internal friction, and dilatometry in the alloys with annealed and quenched initial structure allowed to conclude that when heated up to 600 °C the phase composition of the alloys is almost the same (ferrite + cementite) but the microstructure is different.

A sharp decrease in E_d and G_d of both the initially annealed and initially quenched steel was observed on heating above 750 °C, revealing low elastic stability of the ferrite and austenite lattices at the onset of the α(BCC) $\rightarrow$ γ(FCC) phase transformation. The observed slowing down of the intensive reduction of the dynamic elastic moduli, above 850 °C, is explained by the processes of further development of the $\alpha \rightarrow \gamma$ phase transformation and stabilization of the austenitic phase, with an increase in the elastic stability of its lattice, but the thermal expansion on heating slows down the growth of the elastic moduli of austenite with its further heating.

In the previously quenched alloy, the processes of $\alpha \rightarrow \gamma$ transformation, carbon dissolution, and austenite stabilization are expected to be accomplished faster than in the annealed sample due to accelerated diffusion in the refined sorbite/spheroidite structure, formed from decomposed martensite. The phase transformations between thermodynamically stable phases are accompanied by anomalous behavior of E_d, G_d, and μ and high values of Q^{-1} in the investigated steel in the range 650–900 °C during heating and cooling.

Temperature-dependence plots of the elastic properties (elastic moduli E and G, Poisson's ratio, μ) and of coefficient of expansion obtained in this work on annealed and quenched AISI 4130 are useful to quantify fundamental aspects for the structural analysis of the low-alloy Cr-Mo carbon steel.

These results are relevant for new designs/constructions and for the determination of the temperature regime for their higher performance (mechanical resistance). In addition, the obtained results of the temperature dependence of the elastic moduli and the critical intervals of the softening of the crystal structure due to phase transformations might be of great importance for the selection of economy modes and parameters of its easier deformation during the conformation.

4. Conclusions

The structure and the values of the dynamic moduli E_d and G_d, as well as the Poisson's ratio, μ, and the damping expressed by the internal friction (Q^{-1}), have been determined for annealed and water-quenched AISI 4130 steel by means of the IET approach, at room temperature and during heating to 900 °C and cooling.

1. It was shown that the annealed state of the AISI 4130 steel exhibited a microstructure composed of ferrite + pearlite grains. The E_d and G_d values were determined as 204.6 GPa and 80.5 GPa, respectively, with Poisson's ratio of 0.271. On the other hand, the quenched state of the AISI 4130 steel, with a microstructure composed of martensite and retained austenite, exhibited E_d and G_d values of 193.8 GPa and 78.1 GPa, respectively, with a Poisson's coefficient of 0.273.
2. During the heating cycle, the annealed AISI 4130 steel exhibited a roughly linear decrease for the E_d and G_d in the range from 25 °C to 600 °C. The E_d and G_d modules decreased up to ~167.4 GPa and ~65.1 GPa. In the same range, the slope for the E_d(T) curve was -0.0817 GPa·°C^{-1} whereas the slope for the G_d(T) curve was -0.0332 GPa·°C^{-1}. Poisson's ratio increased from 0.271 to 0.29, while the material expanded linearly with a CTE equal to +1.83 × 10^{-3} °C^{-1}. The measured damping was low, with Q^{-1} varying in the range 0.09 × 10^{-2} to 0.15 × 10^{-2}, with a small increase with a peak up to 0.53 × 10^{-2} centered at ~300 °C, which emerged from internal stress relief.
3. Regarding the quenched state, in the range from 30 °C to 600 °C during the heating cycle, the E_d and G_d modules also decrease linearly to values up to ~158.8 GPa and ~62.2 GPa, respectively. In the same range, the slope for the E_d(T) curve was -0.075 GPa·°C^{-1} whereas the slope for the G_d(T) curve was -0.0308 GPa·°C^{-1}. Poisson's ratio increased very slightly from 0.271 to 0.277, while the material expanded linearly with a non-linear CTE due to metastable phase (martensite and retained austenite) transformations and decomposition. Due to these phase transformations and decomposition, a significant damping peak of 2 × 10^{-2} was observed in the 200–500 °C range.
4. During the heating cycle from 600 °C, the E_d of annealed and quenched states substantially decreased. From 750 to 820 °C, when the material underwent dilatometric compression with the formation of austenite, the E_d sharply decreased (up to 127.5 GPa for the annealed state and 116.2 GPa for the quenched state) and with a greater slope (-0.2822 GPa·°C^{-1} for the annealed state and -0.2752 GPa·°C^{-1} for the quenched state). Above ~710 °C, Poisson's ratio exhibited anomalous values, and the material showed high Q^{-1} values (up to 18 × 10^{-2}). Taking these into account, an unstable state during the phase transition ($\alpha + Fe_3C \rightarrow \gamma$) was verified.
5. From 820 °C to 900 °C, the E_d decreased up to 112.7 GPa in the annealed steel and 108.7 GPa in the quenched steel. However, a small slope of -0.14653 GPa·°C^{-1} was observed for the annealed state compared to the quenched state (-0.098 GPa·°C^{-1}).

This perhaps indicates the interaction of two opposite factors—thermal expansion with increased lattice parameters and the increased thermodynamic stability of the austenitic phase at temperatures above the critical range for the phase transformation. However, the thermal factor was dominant.

6. During the cooling cycle, from 900 °C to 650 °C, E_d and G_d in both alloys increased non-linearly in the range of phase transformations ($\gamma \rightarrow \alpha \rightarrow \alpha + Fe_3C$). In addition, a high value of Q^{-1} ~15×10^{-2} and anomalous values of Poisson's ratio were observed. In the range from 850 to 650 °C, the E_d increased from 114.7 to 150.6 GPa with a slope for the E_d(T) curve of 0.17908 GPa·°C^{-1}, for the annealed state, and from 107.3 GPa to 145.7 GPa, with a slope for the E_d(T) curve of 0.1906 GPa·°C^{-1}, for the quenched state. From 650 °C, Poisson's ratio stabilized and exhibited values in the range of 0.27 to 0.273, whereas Q^{-1} exhibited low values. The E_d and G_d increased non-linearly up to 400 °C. Otherwise, from 400 °C to RT, the E_d and G_d increased linearly with an angular coefficient of +0.68 GPa·°C^{-1} (E_d) and +0.0273 GPa·°C^{-1} (G_d), reaching E_d = 202.9 GPa and G_d = 79.2 GPa in the annealed state and E_d = 200.059 GPa and G_d = 78.59 GPa in the quenched state.
7. As previously stated, despite the high application of the AISI 4130 steel, as far as the authors are aware, this is the first study on the E_d, G_d, μ, and Q^{-1} during the temperature increase using the IET. In some applications, understanding the material behavior in high temperatures is useful. Therefore, the current work is appealing and relevant to new engineering designs using such an alloy.

Author Contributions: Conceptualization, L.A.M.; methodology, L.A.M. and E.C.P.; software, H.A.; formal analysis, L.A.M., E.C.P. and H.A.; investigation, L.A.M., E.C.P. and H.A.; resources, L.A.M., E.C.P. and S.N.M.; data curation, L.A.M., E.C.P., and H.A.; writing—original draft preparation, L.A.M. and E.C.P.; writing—review and editing, L.A.M., E.C.P., N.A.P. and S.N.M.; visualization, L.A.M.; supervision, L.A.M.; project administration, L.A.M.; funding acquisition, L.A.M. and E.C.P. All authors have read and agreed to the published version of the manuscript.

Funding: This research did not receive any specific funding.

Data Availability Statement: The data presented in this study are available on request from the corresponding author.

Acknowledgments: This study was financed in part by the Coordenação de Aperfeiçoamento de Pessoal de Nível Superior—Brazil (CAPES)—Finance Code 001. The authors are grateful for the support given to researchers by MEC, FAPERJ, CAPES, and CNPq. Special thanks to technicians Silvio Gonçalves Mendes, Geovana Girondi, Gabriel Valeriolete, from the Advanced Materials Laboratory UENF, Campos dos Goytacazes, RJ, and to technician Leandro Martins de Oliveira, from COPPE-UFRJ, Rio de Janeiro, for their support in carrying out the metallographic preparation, SEM, CM, and XRD.

Conflicts of Interest: The authors declare no conflict of interest. The funders had no role in the design of the study; in the collection, analyses, or interpretation of data; in the writing of the manuscript, or in the decision to publish the results.

References

1. Ashby, M.F. *Materials Selection in Mechanical Design*, 2nd ed.; Buttereorth Heinemann: Oxford, UK, 1999; ISBN 0750643579.
2. Askeland, D.R.; Wright, W.J. *The Science and Engineering of Materials*, 7th ed.; Cengage Learning: Boston, MA, USA, 2016; ISBN 978-1-350-07676-1.
3. Neto, F.S.; Neves, D.; Silva, O.M.M.; Lima, M.S.F.; Abdalla, A.J. An analysis of the mechanical behavior of AISI 4130 steel after TIG and laser welding process. *Procedia Eng.* **2015**, *114*, 181–188. [CrossRef]
4. Mosayebi, A.; Soleimani, M.; Mirzadeh, H.; Dehghanian, C. Tempering Kinetics and Corrosion Resistance of Quenched and Tempered AISI 4130 Medium Carbon Steel. *Mater. Corros.* **2021**, *72*, 1808–1812. [CrossRef]
5. Tuttle, R. Comparison of Rare Earth Refinement in 4130 and HY100. *Metals* **2021**, *11*, 540. [CrossRef]
6. Casalino, G.; Moradi, M.; Moghadam, M.K.; Khorram, A.; Perulli, P. Experimental and numerical study of AISI 4130 steel surface hardening by pulsed Nd: YAG laser. *Materials* **2019**, *12*, 3136. [CrossRef]
7. Khaksar, L.; Shirokoff, J. Effect of Elemental Sulfur and Sulfide on the Corrosion Behavior of Cr-Mo Low Alloy Steel for Tubing and Tubular Components in Oil and Gas Industry. *Materials* **2017**, *10*, 430. [CrossRef]

8. *Thomas*, a Xometry Company. Available online: https://www.thomasnet.com/articles/metals-metal-products/all-about-4130-steel-properties-strength-and-uses/ (accessed on 5 May 2023).
9. MatWeb–Material Properties Date. Available online: https://www.matweb.com/search/ (accessed on 5 May 2023).
10. Pollard, H.E. Studies of the Dynamic Elastic Behavior of Bounded Solids by Their Response to Mechanical Impulses. Ph.D. Thesis, The University of South Wales, Kensington, Australia, 1962. Available online: https://unsworks.unsw.edu.au/bitstreams/b8ed1f36-7784-4e26-8691-d2efaf707efd/download (accessed on 5 May 2023).
11. Franco, E.E.; Meza, J.M.; Buiochi, F. Measurement of elastic properties of materials by the ultrasonic through-transmission technique. *Dyna* **2011**, *78*, 58–64. Available online: http://www.scielo.org.co/scielo.php?script=sci_arttext&pid=S0012-73532011000400007 (accessed on 5 May 2023).
12. Niutta, C.B.; Tridello, A.; Belingardi, G.; Paolino, D.S. Nondestructive determination of local material properties of laminated composites with the impulse excitation technique. *Compos. Struct.* **2021**, *262*, 113607. [CrossRef]
13. Otani, L.B.; Pereira, A.H.A.; Melo, J.D.D.; Amico, S.C. Determinação dos Módulos Elásticos de Compósitos Empregando a Técnica de Excitação por Impulso. Report Number: ITC-06/ATCP, Vers.1.5 2022. Available online: http://sonelastic.com/images/downloads/ITC-06-IET-MOE-Compósitos-v1.4.pdf (accessed on 5 May 2023).
14. Niutta, C.B. Enhancement of a New Methodology Based on the Impulse Excitation Technique for the Nondestructive Determination of Local Material Properties in Composite Laminates. *Appl. Sci.* **2021**, *11*, 101. [CrossRef]
15. Montecinos, S.; Tognana, S.; Salgueiro, W. Determination of the Young's modulus in CuAlBe shape memory alloys with different microstructures by impulse excitation technique. *Mater. Sci. Eng. A* **2016**, *676*, 121–127. [CrossRef]
16. Popov, I.I.; Shitikova, M.V. Impulse excitation technique and its application for identification of material damping: An overview. *IOP Conf. Ser. Mater. Sci. Eng.* **2020**, *962*, 022025. [CrossRef]
17. Standard Test Method for Dynamic Young's Modulus, Shear Modulus, and Poisson's Ratio by Impulse Excitation of Vibration. ASTM International: West Conshohocken, PA, USA, 2022. Available online: https://www.astm.org/e1876-21.html (accessed on 5 May 2023).
18. Meyers, M.A.; Chawla, K.K. *Mechanical Behavior of Materials*, 2nd ed.; Cambridge University Press: Cambridge, UK, 2008; ISBN 978-0-521-86675-0.
19. Lindgren, L.E.; Back, J.G. Elastic properties of ferrite and austenite in low alloy steels versus temperature and alloying. *Materialia* **2019**, *5*, 100193. [CrossRef]
20. Medved, A.I.; Bryukhanov, A.E. The variation of Young's modulus and the hardness with tempering of some quenched chromium steels. *Met. Sci. Heat Treat.* **1969**, *11*, 706–708. [CrossRef]
21. Łukaszek-Sołek, A.; Śleboda, T.; Lisiecki, Ł.; Krawczyk, J. Hot Deformation Behavior of 4130 High-Strength Steel. *Materials* **2022**, *15*, 7817. [CrossRef]
22. Tripathy, H.; Hajra, R.N.; Sudha, C.; Raju, S.; Saibaba, S. Measurement of high temperature elastic moduli of an 18Cr-9Ni-2.95 Cu-0.58 Nb-0.1 C (Wt%) austenitic stainless steel. *AIP Conf. Proc.* **2018**, *1951*, 020009. [CrossRef]
23. Zener, C. Contributions to the theory of beta-phase alloys. *Phys. Rev.* **1947**, *71*, 846. [CrossRef]
24. Gefen, Y.; Rosen, M. Behaviour of the elastic and anelastic properties of Au-47 · 5 at.% Cd in the vicinity of the cubic-orthorhombic phase transformation. *Philos. Mag.* **1972**, *26*, 727–736. [CrossRef]
25. Kuriyaki, H.; Fukami, T.; Mase, S. Martensitic Transformation in $In_{1-x}Tl_x$ Alloys. *J. Phys. Soc. Jpn.* **1985**, *54*, 989–997. [CrossRef]
26. Sugimoto, K.; Mori, T.; Shiode, S. Effect of Composition on the Internal Friction and Young's Modulus in γ Phase Mn-Cu Alloys. *Met. Sci. J.* **1973**, *7*, 103–108. [CrossRef]
27. Nakanishi, N. Lattice softening and the origin of SME. In *Shape Memory Effects in Alloys*; Perkins, J., Ed.; Metallurgical Society of AIME. Plenum Press: New York, NY, USA; London, UK, 1975; pp. 147–1776.
28. Matlakhova, L.A.; Belousov, O.K.; Palii, N.A. *Elastic Modulus and Structure Changes in TiNi during SME and RSME*; Lambert Academic Publishing: Riga, Latvia, 2018; ISBN 978-6139859375.
29. Lobodyuk, V.; Estrin, E.I. *Martensitic Transformations*; Cambridge International Science Publishing Ltd.: Cambridge, UK, 2014; ISBN -13: 978-1-907343-99-5.
30. Maki, T. Ferrous shape memory alloys. In *Shape Memory Materials*; Otsuka, K., Wayman, C.M., Eds.; Cambridge University Press: Cambridge, UK, 1998; pp. 117–132, ISBN 052144487X, 9780521444873.
31. Fukuhara, M.; Sanpei, A. Elastic moduli and internal friction of low carbon and stainless steels as a function of temperature. *ISIJ Int.* **1993**, *33*, 508–512. [CrossRef]
32. Pučkár, A. *Internal Friction of Materials*; Cambridge International Science Publishing: Cambridge, UK, 2001; ISBN 1 89836 509.
33. Blanter, M.S.; Golovin, I.S.; Neuhauser, H.; Sinning, H.R. *Internal Friction in Metallic Materials—A Handbook*; Springer: Berlin/Heidelberg, Germany, 2007; ISBN 978-3-540-68758-0. [CrossRef]
34. Heidary, O.; Mirzaee, O.; Raouf, A.H.; Borhani, E. UP-quenched SAE 4130 steel: Mechanical properties assessment and bainite formation. *Mater. Sci. Eng. A* **2020**, *787*, 139479. [CrossRef]
35. Bultel, H.; Vogt, J.B. Influence of heat treatment on fatigue behaviour of 4130 AISI steel. *Procedia Eng.* **2010**, *2*, 917–924. [CrossRef]
36. Moravec, J.; Mičian, M.; Málek, M.; Švec, M. Determination of CCT Diagram by Dilatometry Analysis of High-Strength Low-Alloy S960MC Steel. *Materials* **2022**, *15*, 4637. [CrossRef] [PubMed]
37. Owen, E.A.; Williams, G.I. A low-temperature X-ray camera. *J. Sci. Instrum.* **1954**, *31*, 49. [CrossRef]

38. Weissmann, S. (Ed.) *Search Manual for Selected Powder Diffraction Data for Metals and Alloys*; JCPDS International Center for Diffraction Data: Swarthmore, PA, USA, 1978.
39. Fruchart, D.; Chaudouet, P.; Fruchart, R.; Rouault, A.; Senateur, J.P. Etudes structurales de compose´s de type ce´mentite: Effet de l'hydrogene sur Fe3C suivi par diffraction neutronique. Spectrome´trie Mossbauer sur $FeCo_2B$ et Co_3B dope´s au ^{57}Fe. *J. Solid State Chem.* **1984**, *51*, 246–252. [CrossRef]
40. Dann, J.N.; Huang, T.C.; Mueller, M.H.; Wallace, P.L.; Weissmann, S.; Calvert, L.D. A New XRD tool for Metallurgical Research: ICDD's Metals & Alloys Indexes. *Adv. X-Ray Anal.* **1993**, *37*, 109–115. [CrossRef]
41. Samvel'yan, R.G.; Abovyan, E.S.; Agbalyan, S.G.; Manukyan, N.N.; Sakanyan, M.S. X-ray diffraction examination of the process of thermal stabilization of powder thermal bimetals. *Sov. Powder Metall. Met. Ceram.* **1991**, *30*, 606–609. [CrossRef]
42. Pereloma, E.; Edmonds, D.V. (Eds.) Volume 2: Diffusionless Transformations, High Strength Steels, Modelling and Advanced Analytical Techniques. In *Phase Transformations in Steels*; Woodhead Publishing Limited: Cambridge, UK, 2012; ISBN 978-1-84569-971-0.
43. Nishiyama, Z. *Martensitic Transformation*; Fine, M.E., Meshii, M., Wayman, C.M., Eds.; Academic Press, Inc.: New York, NY, USA, 1978; ISBN 0125198507.
44. Graça, S.; Colaço, R.; Carvalho, P.A.; Vilar, R. Determination of dislocation density from hardness measurements in metals. *Mater. Lett.* **2008**, *62*, 3812–3814. [CrossRef]
45. Ameri, A.A.; Elewa, N.N.; Ashraf, M.; Escobedo-Diaz, J.P. General methodology to estimate the dislocation density from microhardness measurements. *Mater. Charact.* **2017**, *131*, 324–330. [CrossRef]
46. Maleki, M.; Mirzadeh, H.; Zamani, M. Effect of Intercritical Annealing on Mechanical Properties and Work-Hardening Response of High Formability Dual Phase Steel. *Steel Res. Int.* **2018**, *89*, 1700412. [CrossRef]
47. Han, K.; van Genderen, M.J.; Böttger, A.; Zandbergen, H.W.; Mittemeijer, E.J. Initial Stages of Fe-C Martensite Decomposition. *Philos. Mag. A* **2001**, *81*, 741–757. [CrossRef]
48. Ciuffini, A.F.; Barella, S.; Di Cecca, C.; Gruttadauria, A.; Mapelli, C.; Mombelli, D. Isothermal Austenite–Ferrite Phase Transformations and Microstructural Evolution during Annealing in Super Duplex Stainless Steels. *Metals* **2017**, *7*, 368. [CrossRef]
49. San Martín, D.; Rivera-Díaz-del-Castillo, P.E.J.; García-de-Andrés, C. In Situ Study of Austenite Formation by Dilatometry in a Low Carbon Microalloyed Steel. *Scr. Mater.* **2008**, *58*, 926–929. [CrossRef]
50. De Andres, C.G.; Caballero, F.G.; Capdevila, C.; Álvarez, L.F. Application of dilatometric analysis to the study of solid–solid phase transformations in steels. *Mater. Charact.* **2002**, *48*, 101–111. [CrossRef]
51. ASM International Handbook Committee. *ASM Handbook Volume 04-Heat Treating*; ASM International: Geauga County, OH, USA, 1991. Available online: https://app.knovel.com/kn/resources/kpASMHVHT3/toc (accessed on 5 May 2023).
52. Atkins, M. *Atlas of Continuous Cooling Transformation Diagrams for Engineering Steels*; American Society for Metals: Metals Park, OH, USA, 1980.
53. Zhou, Z.; Zhu, X. Anomalous temperature dependence of modulus in water-cooled beta Ti-Mo-based alloys. *Mater. Lett.* **2023**, *341*, 134181. [CrossRef]
54. *ASTM E2001-18*; Guide for Resonant Ultrasound Spectroscopy for Defect Detection in Both Metallic and Non-Metallic Parts. ASTM International: West Conshohocken, PA, USA, 2018. [CrossRef]
55. Porter, D.A.; Easterling, K.E.; Sherif, M.Y. *Phase Transformations in Metals and Alloys*, 3rd ed.; Porter, D.A., Easterling, K.E., Sherif, M.Y., Eds.; CRC Press: Boca Raton, FL, USA, 2009; ISBN 9781420062106.
56. Mott, P.H.; Roland, C.M. Limits to Poisson's ratio in isotropic materials. *Phys. Rev. B* **2009**, *80*, 132104. [CrossRef]
57. Gercek, H. Poisson's ratio values for rocks. *Int. J. Rock Mech. Min. Sci.* **2007**, *44*, 1–13. [CrossRef]
58. Goldstein, R.V.; Gorodtsov, V.A.; Lisovenko, D.S. Auxetic mechanics of crystalline materials. *Mech. Solids* **2010**, *45*, 529–545. [CrossRef]
59. Lakes, R.; Wojciechowski, K.W. Negative compressibility, negative Poisson's ratio, and stability. *Phys. Status Solidi* **2008**, *245*, 545–551. [CrossRef]
60. Lipiński, T.; Wach, A. The effect of fine non-metallic inclusions on the fatigue strength of structural steel. *Arch. Metall. Mater.* **2015**, *60*, 65–69. [CrossRef]
61. Ye, X.; Zheng, H.; Zhang, G.; Chang, Z.; Zheng, Z.; Huang, Z.; Gao, X.; Su, G. In Situ Observation of Retained Austenite Transformation in Low-Carbon Micro-Alloyed Q&P Steels. *Crystals* **2023**, *13*, 351. [CrossRef]
62. Jiles, D.C. The effect of compressive plastic deformation on the magnetic properties of AISI 4130 steels with various microstructures. *J. Phys. D Appl. Phys.* **1988**, *21*, 1196. [CrossRef]